

Epitaxial growth of trilayer graphene moiré superlattice

Yalong Yuan(袁亚龙), Yanbang Chu(褚衍邦), Cheng Hu(胡成), Jinpeng Tian(田金朋), Le Liu(刘乐), Fanfan Wu(吴帆帆), Yiru Ji(季怡汝), Jiaojiao Zhao(赵交交), Zhiheng Huang(黄智恒), Xiaozhou Zan(昝晓洲), Luojun Du(杜罗军), Kenji Watanabe, Takashi Taniguchi, Dongxia Shi(时东霞), Zhiwen Shi(史志文), Wei Yang(杨威), and Guangyu Zhang(张广宇)

Citation: Chin. Phys. B, 2023, 32 (**7**): 077304. DOI: 10.1088/1674-1056/accdc8
Journal homepage: http://cpb.iphy.ac.cn; http://iopscience.iop.org/cpb

What follows is a list of articles you may be interested in

Superconductivity in epitaxially grown $LaVO_3/KTaO_3(111)$ heterostructures

Yuan Liu(刘源), Zhongran Liu(刘中然), Meng Zhang(张蒙), Yanqiu Sun(孙艳秋), He Tian(田鹤), and Yanwu Xie(谢燕武)

Chin. Phys. B, 2023, 32 (**3**): 037305. DOI: 10.1088/1674-1056/acac1b

Precisely controlling the twist angle of epitaxial MoS_2/graphene heterostructure by AFM tip manipulation

Jiahao Yuan(袁嘉浩), Mengzhou Liao(廖梦舟), Zhiheng Huang(黄智恒), Jinpeng Tian(田金朋), Yanbang Chu(褚衍邦), Luojun Du(杜罗军), Wei Yang(杨威), Dongxia Shi(时东霞), Rong Yang(杨蓉), and Guangyu Zhang(张广宇)

Chin. Phys. B, 2022, 31 (**8**): 087302. DOI: 10.1088/1674-1056/ac720e

Surface states modulated exchange interaction in Bi_2Se_3/thulium iron garnet heterostructures

Hai-Bin Shi(石海滨), Li-Qin Yan(闫丽琴), Yang-Tao Su(苏仰涛), Li Wang(王力), Xin-Yu Cao(曹昕宇), Lin-Zhu Bi(毕林竹), Yang Meng(孟洋), Yang Sun(孙阳), and Hong-Wu Zhao(赵宏武)

Chin. Phys. B, 2020, 29 (**11**): 117302. DOI: 10.1088/1674-1056/abbbdf

High crystalline quality of SiGe fin fabrication with Si-rich composition area using replacement fin processing

Ying Zan(昝颖), Yong-Liang Li(李永亮), Xiao-Hong Cheng(程晓红), Zhi-Qian Zhao(赵治乾), Hao-Yan Liu(刘昊炎), Zhen-Hua Hu(吴振华), An-Yan Du(都安彦), Wen-Wu Wang(王文武)

Chin. Phys. B, 2020, 29 (**8**): 087303. DOI: 10.1088/1674-1056/ab973e

Epitaxial fabrication of monolayer copper arsenide on Cu(111)

Shuai Zhang(张帅), Yang Song(宋洋), Jin Mei Li(李金梅), Zhenyu Wang(王振宇), Chen Liu(刘晨), Jia-Ou Wang(王嘉鸥), Lei Gao(高蕾), Jian-Chen Lu(卢建臣), Yu Yang Zhang(张余洋), Xiao Lin(林晓), Jinbo Pan(潘金波), Shi Xuan Du(杜世萱), Hong-Jun Gao(高鸿钧)

Chin. Phys. B, 2020, 29 (**7**): 077301. DOI: 10.1088/1674-1056/ab8db3

Epitaxial growth of trilayer graphene moiré superlattice

Yalong Yuan(袁亚龙)[1,2], Yanbang Chu(褚衍邦)[1,2], Cheng Hu(胡成)[3,4], Jinpeng Tian(田金朋)[1,2], Le Liu(刘乐)[1,2], Fanfan Wu(吴帆帆)[1,2], Yiru Ji(季怡汝)[1,2], Jiaojiao Zhao(赵交交)[1,2], Zhiheng Huang(黄智恒)[1,2], Xiaozhou Zan(昝晓洲)[1,2], Luojun Du(杜罗军)[1,2], Kenji Watanabe[5], Takashi Taniguchi[6], Dongxia Shi(时东霞)[1,2,3], Zhiwen Shi(史志文)[3,4], Wei Yang(杨威)[1,2,7,‡], and Guangyu Zhang(张广宇)[1,2,7,†]

[1] *Beijing National Laboratory for Condensed Matter Physics and Institute of Physics, Chinese Academy of Sciences (CAS), Beijing* 100190, *China*
[2] *School of Physical Sciences, University of Chinese Academy of Sciences, Beijing* 100190, *China*
[3] *Key Laboratory of Artificial Structures and Quantum Control (Ministry of Education), School of Physics and Astronomy, Shanghai Jiao Tong University, Shanghai* 200240, *China*
[4] *Collaborative Innovation Center of Advanced Microstructures, Nanjing* 210093, *China*
[5] *Research Center for Functional Materials, National Institute for Materials Science*, 1-1 *Namiki, Tsukuba* 305-0044, *Japan*
[6] *International Center for Materials Nanoarchitectonics, National Institute for Materials Science*, 1-1 *Namiki, Tsukuba* 305-0044, *Japan*
[7] *Songshan Lake Materials Laboratory, Dongguan* 523808, *China*

(Received 23 February 2023; revised manuscript received 12 April 2023; accepted manuscript online 18 April 2023)

The graphene-based moiré superlattice has been demonstrated as an exciting system for investigating strong correlation phenomenon. However, the fabrication of such moiré superlattice mainly relies on transfer technology. Here, we report the epitaxial growth of trilayer graphene (TLG) moiré superlattice on hexagonal boron nitride (hBN) by a remote plasma-enhanced chemical vapor deposition method. The as-grown TLG/hBN shows a uniform moiré pattern with a period of ~ 15 nm by atomic force microscopy (AFM) imaging, which agrees with the lattice mismatch between graphene and hBN. By fabricating the device with both top and bottom gates, we observed a gate-tunable bandgap at charge neutral point (CNP) and displacement field tunable satellite resistance peaks at half and full fillings. The resistance peak at half-filling indicates a strong electron–electron correlation in our grown TLG/hBN superlattice. In addition, we observed quantum Hall states at Landau level filling factors $\nu = 6, 10, 14, \ldots$, indicating that our grown trilayer graphene has the ABC stacking order. Our work suggests that epitaxy provides an easy way to fabricate stable and reproducible two-dimensional strongly correlated electronic materials.

Keywords: epitaxial growth, ABC-TLG/hBN moiré superlattice, electron correlations

PACS: 73.21.Cd, 81.15.Gh, 72.80.Vp, 73.50.–h **DOI:** 10.1088/1674-1056/accdc8

Graphene-based moiré superlattices have been demonstrated as ideal flat band systems for investigating correlated physics.[1–19] Among them, a moiré superlattice of ABC stacked trilayer graphene (ABC-TLG),[7,20–22] by aligning its lattice with the hexagonal boron nitride (hBN) substrate, has attracted considerable attention. As a matter of fact, the band structure of ABC-TLG itself is quite flat with field tunable van Hove singularities (vHS) near the band edge, contributing to various symmetry broken metalic phases and superconductivity.[23,24] Moreover, with the introducing of a long wavelength periodic potential in ABC-TLG/hBN hetero moiré superlattice, isolated flat moiré bands near the charge neutral point are generated at finite displacement field, which eventually leads to the discovery of correlated insulators, superconductivity, and anomalous quantum Hall effect in this system.[7,20–22] Compared to the twisted bilayer graphene, ABC-TLG/hBN moiré superlattice have more freedom on the twist angle control. Thus far, ABC-TLG/hBN moiré superlattice is highly relied on the complicated pick-up transferring, and a technique capable of fabricating moiré superlattice for easy production with a large scale is high demanded.

In this work, we directly obtain TLG/hBN moiré superlattice by epitaxy. The epitaxial grown trilayer graphene and the hBN substrate are aligned, giving a moiré period of ~ 15 nm. We fabricate the epitaxial TLG into devices with a dual gate configuration. The transport results show that the TLG has the characteristics of ABC stacking order, supported by the presence of a band gap of 1.2 meV at the charge neutral point and the quantum Hall states with Landau levels filling factors of of $\nu = 6, 10, 14, \ldots$. In addition, we observe a resistance peak at half filling at a finite displacement field, implying the presence of strongly correlation in our epitaxial grown ABC-TLG/hBN moiré superlattice.

Figure 1(a) is a schematic diagram of the epitaxial trilayer graphene on hBN substrates, and figure 1(b) is the resulted moiré superlattice structure measured from atomic force microscopy (AFM) imaging. The growth of TLG is carried out in a remote plasma-enhanced chemical vapour deposition system (r-PECVD). Before growth, hBN flakes are mechanically exfoliated onto a 300-nm-thick SiO_2/Si. During the growth,

†Corresponding author. E-mail: gyzhang@iphy.ac.cn
‡Corresponding author. E-mail: wei.yang@iphy.ac.cn

© 2023 Chinese Physical Society and IOP Publishing Ltd

methane (CH_4) is used as the feed gas, with a low growth pressure of 0.2 Torr (1 Torr = 1.33322×10^5 Pa). Assisted by the plasma technique, methane can be decomposed into various reactive radicals, from which the carbon or hydrocarbon radicals allowing the nucleation and growth of graphene and the hydrogen radicals can remove amorphous carbon and ensure sp^2 carbon growth.[25–27] At an optimal temperature (T) of $\sim 500\,^{\circ}$C, we can achieve epitaxial growth of single-domain graphene as previously reported.[28–30] Figures 1(c)–1(f) show the epitaxy of TLG/hBN moiré superlattice at different growth stages. At the nucleation stage, monolayer graphene islands are randomly formed on the hBN surface. As carbon atoms are continuously deposited onto the surface, the existing nuclei grow and connect (Fig. 1(c)), which eventually produces a continuous and uniform graphene film with second-layer graphene islands grown on top (Fig. 1(d)). By extending the growth time, the second layer graphene also forms a continuous bilayer graphene film topped with islands of the third-layer (Fig. 1(e)), which then gradually grow and coalesce to produce a continuous trilayer graphene film with a small amount of the fourth-layer islands on top (Fig. 1(f)). In our epitaxial grown TLG on hBN, we observed a clear moiré pattern with a period of 15 nm using AFM (Fig. 1(b)). The resulted moiré periodicity in TLG/hBN agrees well with that in epitaxial monolayer graphene/hBN moiré superlattice from our previous reports;[28–30] and thus, we attribute the superlattice to the lattice mismatch between TLG and hBN at zero rotation angle.

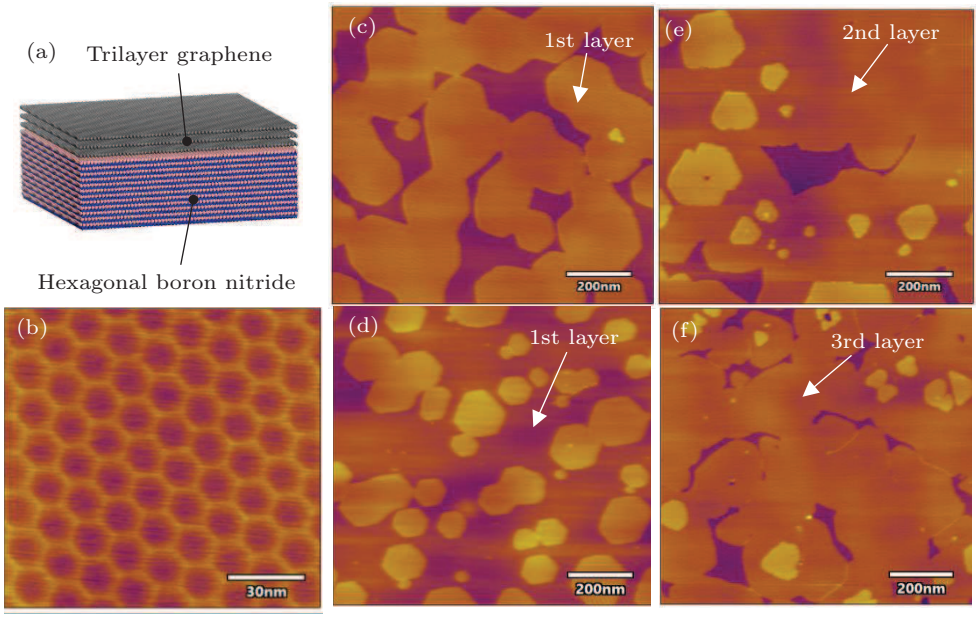


Fig. 1. Epitaxial trilayer graphene growth on hBN. (a) Schematic diagram of epitaxial growth structure. (b) Moiré pattern of epitaxial trilayer graphene/hBN superlattice. (c)–(f) AFM images of as-grown graphene on hBN at different stages including small grains nucleation and coalescence of grains (c), continuous monolayer graphene with some second-layer nuclei on top (d), continuous bilayer graphene with some third-layer nuclei on top (e), and continuous trilayer graphene with some fourth-layer nuclei on top (f).

We now turn to the electrical properties of the epitaxial trilayer graphene grown on hBN. Another hBN flake was stacked on the TLG/hBN structure for encapsulation and as a top-gate dielectric. The device was then etched into a Hall bar structure using standard electron-beam lithography techniques, and Cr/Au was deposited for contacts and top gate electrodes.[31] Our devices have a dual gate configuration, which allows independent tuning of the carrier density n and displacement field D. Here, $n = (C_{BG}V_{BG} + C_{TG}V_{TG})/e$ and $D = (C_{BG}V_{BG} - C_{TG}V_{TG})/2\varepsilon_0$, where C_{BG} (C_{TG}) is the geometrical capacitance per area for bottom (top) gate, e is the electron charge, and ε_0 is the vacuum permittivity. All measurements are done at $T = 1.8$ K unless stated otherwise.

The measured the longitudinal resistance (R_{xx}) as a function of the bottom gate (V_{BG}) and top gate (V_{TG}) is shown in Fig. 2(a). We can observe the obvious resistance peak at the charge neutral point (CNP), and the resistance increases with the increase of the displacement field D. Figure 2(d) shows the temperature dependence of $R_{xx}(n)$ at $D = 0$. The resistivity peak at CNP exhibits typical insulating behavior, *i.e.*, R_{xx} increases as T decreases. The extracted thermally activated bandgap (Δ) at CNP is of 1.2 meV at $D = 0$, and it increases with the increase of D as shown in Fig. 2(f). Trilayer graphene has two stable stacking orders in its natural form: ABA (Bernal) and ABC (rhombohedral). The ABC trilayer graphene is a semiconductor with a gate-tunable band gap, while the ABA trilayer graphene is a gapless semimetal.[32–36] The observations of the gap opening at CNP and its field tunability agree well with transport characteristics of ABC (rhombohedral) stacked TLG.

In addition to the resistance peak at CNP, we also observed the resistance peaks at around $n = \pm 1.92\times10^{12}$ cm^{-2}

in Fig. 2(d). Such resistance peaks become barely discernible at $T > 30$ K, and the temperature dependence also exhibits insulating behavior (as shown in Fig. 2(e)). In principle, similar to the epitaxial graphene/hBN superlattice[28–30] and transferred ABC-TLG/hBN superlattice,[7,20,21] the epitaxial TLG/hBN superlattice would introduce a periodic potential modulation on the TLG, which leads to a reconstruction of the TLG band structure by forming moiré mini-Brillouin zone and moiré Bloch bands. By taking spin and valley degree of freedom into account, it takes 4 electrons (holes) to fully fill the moiré conduction (valence) band. The carrier density at the full filling (n_s) is defined as $n_s = 4/A$, where $A = (\sqrt{3}/2)\lambda^2$ is the area of a moiré unit cell and the λ is the moiré superlattice period. The resistance peaks at $n_s = 1.92 \times 10^{12}$ cm^{-2} gives a moiré superlattice period $\lambda = 15$ nm, which is consistent with the previous AFM results. Therefore, these two peaks correspond to the gap openings at the full fillings of the TLG/hBN moiré superlattice.[28,37]

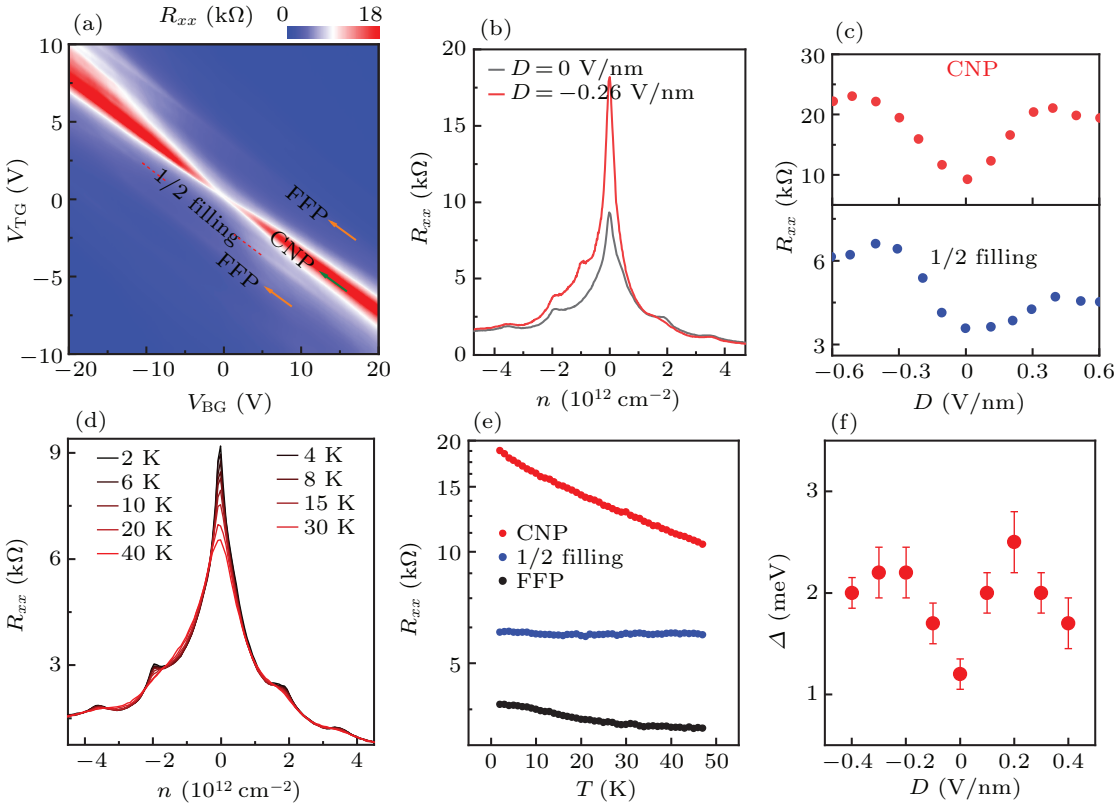


Fig. 2. Transport measurements of trilayer graphene/hBN superlattice. (a) Longitudinal resistivity R_{xx} as a function of top gate V_{TG} and bottom gate V_{BG}. (b) Longitudinal resistivity R_{xx} *versus* carrier density n at $D = 0$ and -0.26 V/nm. (c) Longitudinal resistivity R_{xx} at the charge neutral point (CNP) and 1/2 filling in the hole side tuned by displacement field D. (d) Temperature-dependent longitudinal resistivity R_{xx} *versus* carrier density n at $D = 0$. The resistivity peaks at CNP and full filling point (FFP) exhibit typical insulating behavior where the resistance increases with reduced temperature. (e) Longitudinal resistivity R_{xx} *versus* temperature T at $D = -0.26$ V/nm. The resistance at CNP and FFP decreases with increasing temperature, and the resistance at 1/2 filling varies little with temperature. (f) Thermal activation gaps Δ *versus* displacement fields D at CNP.

Next, we discuss the transfer curve at a nonzero finite displacement field. In addition to the resistance peaks at $n = 0$ and $n = \pm n_s$ that can be observed at all displacement fields, we observe features of half filling resistance peak at high displacement fields in Fig. 2(a). This can be clearer reflected in the transfer curve comparison in Fig. 2(b), where a new resistance peak appears at half filling in the valence band for $D = -0.26$ V/nm and it is featureless for $D = 0$. Similar to that at CNP, the resistance at 1/2 filling increases with the increase of the displacement field strength as shown in Fig. 2(c). Such a resistance peak at 1/2 filling implies strongly correlated states in our grown ABC-TLG/hBN moiré superlattice.[20,22] However, the resistance at 1/2 filling is T insensitive (Fig. 2(e)). By increasing the temperature, the resistance usually increases for metals, while by contrast it decreases for insulators. In this sense, such T insensitive behavior might suggest a coexistence of both metallic and insulating regions in the device. One possible reason lies in the presence of the additional 4th layer graphene domains in the TLG/hBN moiré superlattice. Another possible reason might due to the presence of ABA TLG domains, whose metallic nature prevents a developing of the insulating states at 1/2 filling.

Lastly, we perform magnetic transport measurements for the TLG/hBN moiré superlattice. In a strong perpendicular magnetic field, the two-dimensional electronic system in TLG obeys the Landau quantization and gives quantized Hall conductance $\sigma_{xy} = \nu \times e^2/h$, where ν is the Landau level (LL) filling factor. In graphene multilayer systems, the number of

graphene layers as well as the stacking order determines the characteristics of the Landau level spectrum. According to previous reports, the LLs in ABC trilayer graphene gives Hall plateaus at[32,38] $\sigma_{xy} = \pm(ge^2/h)(n_{\rm LL} + N/2)$ where $N = 3$ is the number of layers, $n_{\rm LL}$ is the LL index, $g = 4$ is the LL degeneracy accounting for spin and valley degrees of freedom, e is the electron charge, and h is Planck's constant. By contrast, the LLs in ABA trilayer graphene can be viewed as a superposition of $\sqrt{B}$-dependent monolayerlike LLs and B-dependent bilayerlike LLs.[38,39] Figure 3(a) shows a color mapping of longitudinal resistance (R_{xx}) as a function of carrier density (n) and magnetic field (B), and the lower panel is a corresponding schematic highlighting the trajectories of the resistance minimum. We can observe a series of Landau fans from CNP that corresponds to the filling factor $\nu = \pm 6, \pm 10, \pm 14, \ldots$ Figure 3(b) shows R_{xx} and Hall conductance σ_{xy} at $B = 9$ T, from which near quantized Hall conductance σ_{xy} and R_{xx} minima are observed at $\nu = \pm 6, \pm 10, \pm 14, \ldots$ Anyway, these magneto transport results do suggest that the epitaxial trilayer graphene has the characteristics of ABC stacking order.

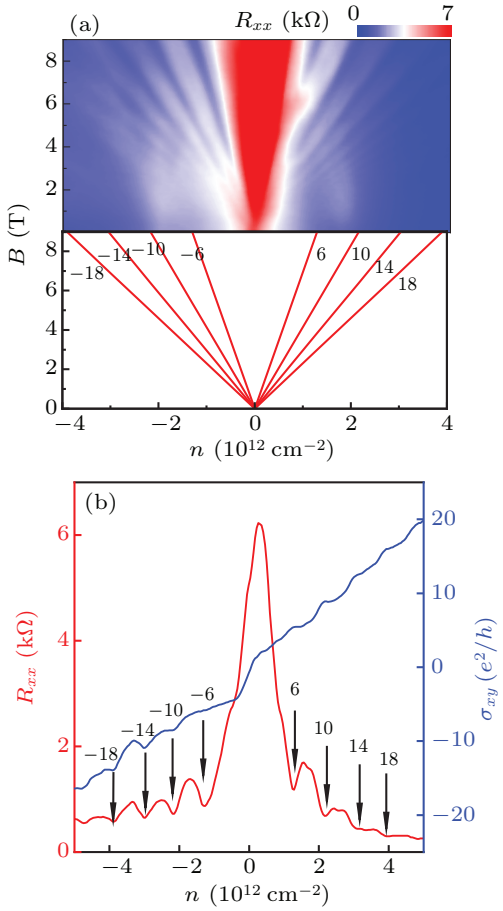


Fig. 3. Shubnikov–de Haas oscillations in our grown trilayer graphene. (a) Top longitudinal resistance R_{xx} as a function of carrier density n and magnetic field B. Bottom, the corresponding schematics that identifies visible Landau level fans. (b) Longitudinal resistance (R_{xx}, red) and Hall conductance (σ_{xy}, blue) *versus* carrier density n at $T = 1.8$ K, $B = 9$ T.

In conclusion, we successfully realized the epitaxy of trilayer graphene/hBN moiré superlattices. The moiré periodicity of ~ 15 nm is stable and uniform, formed due to the lattice mismatch between TLG and hBN with zero twisted angle. The electrical transport measurements in TLG/hBN suggest an ABC stacking order of TLG, supported by the evidences of gate-tunable band gap and Landau levels spectra. We also observed a resistance peak at 1/2 filling, indicating a strong correlation in the epitaxial ABC-TLG/hBN superlattice. Although more efforts are needed to address sample quality issues in future, our work indicates that epitaxy might provide a stable and reproducible new way to obtain moiré superlattice for investigating strong correlated physics.

Acknowledgements

Project supported by the National Key Research and Development Program of China (Grant No. 2020YFA0309600), the National Natural Science Foundation of China (Grant Nos. 61888102, 11834017, and 12074413), the Strategic Priority Research Program of CAS (Grant Nos. XDB30000000 and XDB33000000), and the Key-Area Research and Development Program of Guangdong Province, China (Grant No. 2020B0101340001). K. W. and T. T. acknowledge support from the Elemental Strategy Initiative conducted by the MEXT, Japan (Grant No. JPMXP0112101001), JSPS KAKENHI (Grant Nos. 19H05790, 20H00354, and 21H05233), and A3 Foresight by JSPS.

References

[1] Bistritzer R and MacDonald A H 2011 *Proc. Natl. Acad. Sci. USA* **108** 12233
[2] Cao Y, Fatemi V, Demir A, Fang S, Tomarken S L, Luo J Y, Sanchez-Yamagishi J D, Watanabe K, Taniguchi T, Kaxiras E, Ashoori R C and Jarillo-Herrero P 2018 *Nature* **556** 80
[3] Lu X, Stepanov P, Yang W, Xie M, Aamir M A, Das I, Urgell C, Watanabe K, Taniguchi T, Zhang G, Bachtold A, MacDonald A H and Efetov D K 2019 *Nature* **574** 653
[4] Shen C, Chu Y, Wu Q, Li N, Wang S, Zhao Y, Tang J, Liu J, Tian J, Watanabe K, Taniguchi T, Yang R, Meng Z Y, Shi D, Yazyev O V and Zhang G 2020 *Nat. Phys.* **16** 520
[5] Kim H, Choi Y, Lewandowski C, Thomson A, Zhang Y, Polski R, Watanabe K, Taniguchi T, Alicea J and Nadj-Perge S 2022 *Nature* **606** 494
[6] Park J M, Cao Y, Xia L Q, Sun S W, Watanabe K, Taniguchi T and Jarillo-Herrero P 2022 *Nat. Mater.* **21** 877
[7] Chen G, Sharpe A L, Fox E J, Zhang Y H, Wang S, Jiang L, Lyu B, Li H, Watanabe K, Taniguchi T, Shi Z, Senthil T, Goldhaber-Gordon D, Zhang Y and Wang F 2020 *Nature* **579** 56
[8] Cao Y, Fatemi V, Fang S, Watanabe K, Taniguchi T, Kaxiras E and Jarillo-Herrero P 2018 *Nature* **556** 43
[9] Liu J, Ma Z, Gao J and Dai X 2019 *Phys. Rev. X* **9** 031021
[10] Yankowitz M, Chen S, Polshyn H, Zhang Y, Watanabe K, Taniguchi T, Graf D, Young A F and Dean C R 2019 *Science* **363** 1059
[11] Cao Y, Rodan-Legrain D, Rubies-Bigorda O, Park J M, Watanabe K, Taniguchi T and Jarillo-Herrero P 2020 *Nature* **583** 215
[12] He M, Li Y, Cai J, Liu Y, Watanabe K, Taniguchi T, Xu X and Yankowitz M 2020 *Nat. Phys.* **17** 26
[13] Lisi S, Lu X, Benschop T, *et al.* 2020 *Nat. Phys.* **17** 189
[14] Liu X, Hao Z, Khalaf E, Lee J Y, Ronen Y, Yoo H, Haei Najafabadi D, Watanabe K, Taniguchi T, Vishwanath A and Kim P 2020 *Nature* **583** 221
[15] Polshyn H, Zhu J, Kumar M A, Zhang Y, Yang F, Tschirhart C L, Serlin M, Watanabe K, Taniguchi T, MacDonald A H and Young A F 2020 *Nature* **588** 66

[16] Serlin M, Tschirhart C L, Polshyn H, Zhang Y, Zhu J, Watanabe K, Taniguchi T, Balents L and Young A F 2020 *Science* **367** 900

[17] Park J M, Cao Y, Watanabe K, Taniguchi T and Jarillo-Herrero P 2021 *Nature* **590** 249

[18] Liu L, Zhang S, Chu Y, Shen C, Huang Y, Yuan Y, Tian J, Tang J, Ji Y, Yang R, Watanabe K, Taniguchi T, Shi D, Liu J, Yang W and Zhang G 2022 *Nat. Commun.* **13** 3292

[19] Chu Y, Liu L, Shen C, Tian J, Tang J, Zhao Y, Liu J, Yuan Y, Ji Y, Yang R, Watanabe K, Taniguchi T, Shi D, Wu F, Yang W and Zhang G 2022 *Phys. Rev. B* **106** 035107

[20] Chen G, Jiang L, Wu S, Lyu B, Li H, Chittari B L, Watanabe K, Taniguchi T, Shi Z, Jung J, Zhang Y and Wang F 2019 *Nat. Phys.* **15** 237

[21] Chen G, Sharpe A L, Gallagher P, Rosen I T, Fox E J, Jiang L, Lyu B, Li H, Watanabe K, Taniguchi T, Jung J, Shi Z, Goldhaber-Gordon D, Zhang Y and Wang F 2019 *Nature* **572** 215

[22] Chittari B L, Chen G, Zhang Y, Wang F and Jung J 2019 *Phys. Rev. Lett.* **122** 016401

[23] Zhou H X, Xie T, Ghazaryan A, Holder T, Ehrets J R, Spanton E M, Taniguchi T, Watanabe K, Berg E, Serbyn M and Young A F 2021 *Nature* **598** 429

[24] Zhou H X, Xie T, Taniguchi T, Watanabe K and Young A F 2021 *Nature* **598** 434

[25] Liu D, Yang W, Zhang L, Zhang J, Meng J, Yang R, Zhang G and Shi D X 2014 *Carbon* **72** 387

[26] Zhang L, Ni M, Liu D, Shi D and Zhang G 2012 *J. Phys. Chem. C* **116** 26929

[27] Zhang L, Shi Z, Liu D, Yang R, Shi D and Zhang G 2012 *Nano Res.* **5** 258

[28] Yang W, Chen G, Shi Z, Liu C C, Zhang L, Xie G, Cheng M, Wang D, Yang R, Shi D, Watanabe K, Taniguchi T, Yao Y, Zhang Y and Zhang G 2013 *Nat. Mater.* **12** 792

[29] Yang W, Lu X, Chen G, Wu S, Xie G, Cheng M, Wang D, Yang R, Shi D, Watanabe K, Taniguchi T, Voisin C, Placais B, Zhang Y and Zhang G 2016 *Nano Lett.* **16** 2387

[30] Lu X, Tang J, Wallbank J R, Wang S, Shen C, Wu S, Chen P, Yang W, Zhang J, Watanabe K, Taniguchi T, Yang R, Shi D, Efetov D K, Fal'ko V I and Zhang G 2020 *Phys. Rev. B* **102** 045409

[31] Wang L, Meric I, Huang P Y, Gao Q, Gao Y, Tran H, Taniguchi T, Watanabe K, Campos L M, Muller D A, Guo J, Kim P, Hone J, Shepard K L and Dean C R 2013 *Science* **342** 614

[32] Jhang S H, Craciun M F, Schmidmeier S, Tokumitsu S, Russo S, Yamamoto M, Skourski Y, Wosnitza J, Tarucha S, Eroms J and Strunk C 2011 *Phys. Rev. B* **84** 161408

[33] Bao W, Jing L, Velasco J, Lee Y, Liu G, Tran D, Standley B, Aykol M, Cronin S B, Smirnov D, Koshino M, McCann E, Bockrath M and Lau C N 2011 *Nat. Phys.* **7** 948

[34] Zou K, Zhang F, Clapp C, MacDonald A H and Zhu J 2013 *Nano Lett.* **13** 369

[35] Taychatanapat T, Watanabe K, Taniguchi T and Jarillo-Herrero P 2011 *Nat. Phys.* **7** 621

[36] Craciun M F, Russo S, Yamamoto M, Oostinga J B, Morpurgo A F and Tarucha S 2009 *Nat. Nanotechnol.* **4** 383

[37] Dean C R, Wang L, Maher P, Forsythe C, Ghahari F, Gao Y, Katoch J, Ishigami M, Moon P, Koshino M, Taniguchi T, Watanabe K, Shepard K L, Hone J and Kim P 2013 *Nature* **497** 598

[38] Yuan S, Roldán R and Katsnelson M I 2011 *Phys. Rev. B* **84** 125455

[39] Datta B, Agarwal H, Samanta A, Ratnakar A, Watanabe K, Taniguchi T, Sensarma R and Deshmukh M M 2018 *Phys. Rev. Lett.* **121** 056801